

# The design of GaAs/AlAs resonant tunneling diodes with peak current densities over $2 \times 10^5 \text{ A cm}^{-2}$

E. Wolak,<sup>a)</sup> E. Özbay,<sup>b)</sup> B. G. Park, S. K. Diamond,<sup>c)</sup> David M. Bloom,<sup>b)</sup> and James S. Harris, Jr.

Department of Electrical Engineering, 226 McCullough, Stanford University, Stanford, California 94305-4055

(Received 6 February 1990; accepted for publication 26 November 1990)

A coherent transport model is described which accommodates bandstructure nonparabolicity by using a "local energy parabolic band approximation." The model and a knowledge of its limitations is used to design resonant tunneling diodes in the GaAs/AlAs material system with measured peak current densities of  $2.5(2.8) \times 10^5 \text{ A cm}^{-2}$  concurrent with peak-to-valley ratios as high as 1.8 (3.1) at room temperature (77 K).

## I. INTRODUCTION

Since the initial proposal and fabrication of resonant tunneling diodes (RTDs),<sup>1,2</sup> extensive efforts have been made to improve the current-voltage ( $I$ - $V$ ) characteristics of these devices. Much of this effort has been focused on improving the peak-to-valley current ratios of these structures, and significant progress has been made.<sup>3-6</sup> It has been shown that once a satisfactory peak-to-valley ratio has been achieved, further improvements in device performance must come from lowering the device capacitance and increasing the peak current density of the device.<sup>7,8</sup>

Models of the transport through tunneling structures can provide a useful guide in the design of such devices; this is critical because of the strong dependence of tunneling currents on various device parameters. The valley current, that is the current which occurs at voltages above the resonant current peak, is not well understood in the GaAs/AlAs material system, and historically there has been an apparent empirical tradeoff in the peak-to-valley current ratio and peak current density of this material system.<sup>3</sup> Recently, these limitations have been overcome by working in other materials systems,<sup>3,4,6</sup> however, we concentrate on the GaAs/AlAs material system in this work due to its maturing processing technology and increasing applications.

In this paper, we describe the use of a coherent transport model, combined with a knowledge of its limitations, to design high-current density RTDs in the GaAs/AlAs material system. The coherent model and its predictions are summarized in Sec. II of this paper. The peak current densities for several published results are compared with the model, and the limitations of the applicability of the model are described. In Sec. III, we describe the design, crystal growth, and fabrication of resonant tunneling devices with peak current densities of over  $2 \times 10^5 \text{ A cm}^{-2}$  and an estimated capacitance per unit area of roughly  $100 \text{ nF cm}^{-2}$ . We have optimized the devices without the constraint of symmetry in the doping profile imposed in most

previous RTD structures. One of these devices exhibits the largest difference in  $J_p$  and  $J_v$  (peak and valley current densities, respectively) reported to date in the GaAs/AlAs system. The difference in peak and valley current densities is critical in the figure of merit for high-speed electronic applications.<sup>7,8</sup> Devices with the epitaxial layers described in this paper will be useful in both oscillator and switching applications once the device processing techniques are modified to reduce the series resistance. Furthermore, the concepts of this paper can be applied to the other material systems used for resonant tunneling devices. A summary is given in Sec. IV.

## II. THE MODEL

In this section, we will show that the coherent picture of resonant tunneling can be used as a method of estimating the current density through the quantum potential barriers with certain limitations. Within this picture, electrons are assumed to tunnel through the double barrier structure in a manner described by the single-electron transmission probability function  $|T(E_x, V)|^2$ , thus neglecting scattering effects.<sup>9</sup> We work within the independent electron approximation, and assume that the Hamiltonian in the plane of the heterointerfaces, and perpendicular to it is separable. Furthermore, it is assumed that the electrons before and after the quantum region form a Fermi sea, which can be a good approximation when the cathode is doped sufficiently and any lightly doped spacer layers total less than  $200 \text{ \AA}$  on the cathode side. Once these approximations have been made, the current density through the structure can be approximated as

$$J = \frac{4\pi m^* k T q}{h^3} \int_{E_c}^{\infty} dE_x |T(E_x, V)|^2 \times \ln \left( \frac{1 + \exp[(E_f - E_x)/kT]}{1 + \exp[(E_{fa} - E_x - eV)/kT]} \right), \quad (1)$$

<sup>a)</sup>Currently at the Opto-Electronic Research Laboratories, Matsushita Electric Industrial Co, 3-15 Yagumo-Nakamachi, Moriguchi Osaka 570, Japan.

<sup>b)</sup>With the Edward L. Ginzton Laboratories, Stanford University, Stanford, CA 94305-4085.

<sup>c)</sup>Presently with Tektronics Laboratories, Beaverton, OR 97077.

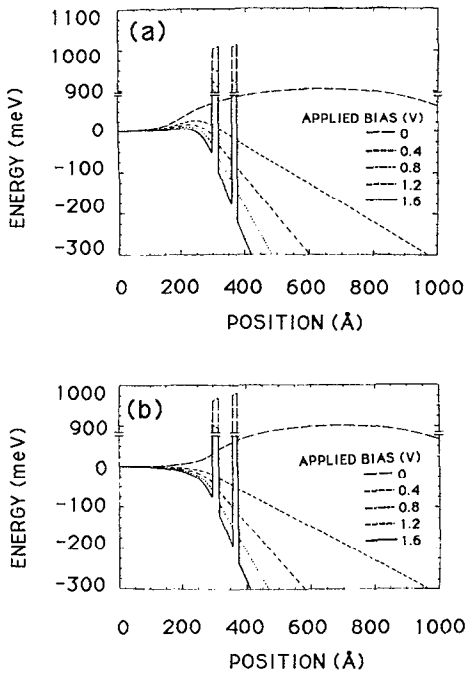


FIG. 1. The conduction-band minimum is shown as a function of position under various bias conditions for devices from Ref. 20 in (a), and without the 100-Å undoped spacer in (b). The use of the 100-Å undoped spacer helps reduce the accumulation region, and is thought to help reduce valley currents.

where  $q$  is the magnitude of the electronic charge,  $m^*$  is the electron effective mass in the cathode,  $h$  is the Planck constant,  $kT$  is the product of the Boltzmann constant and the ambient temperature,  $E_c$  is the energy of the conduction-band minimum in the cathode contact,  $E_f$  is the Fermi energy on the cathode side,  $E_{fa}$  is the Fermi energy on the anode side,  $eV$  is the potential drop between the cathode and anode, and  $|T(E_x, V)|^2$  is the tunneling probability as a function of electron longitudinal energy in the cathode and applied voltage.<sup>1</sup> Given the conditions where the above approximations are valid, we will show agreement between this model and published results within a factor of 2.5 for peak current densities ranging over two orders of magnitude.

We calculate the transmission function  $|T(E_x, V)|^2$  by solving the single-particle Schrödinger equation in the transport direction using only the envelope part of the wave function. Our technique consists of approximating the exact potential energy profile of the double-barrier structure by a sequence of flat steps<sup>10</sup>; to include the effects of band bending in the layers surrounding the RTD in the calculation of the  $I$ - $V$  curves, the potential as a function of position is found using a Poisson equation solver.<sup>11</sup> A solution of the potential as a function of position in the transport direction is shown in Fig. 1. The boundary conditions at each potential step are continuity of the wave function and continuity of electron flux:

$$F_n = F_{n+1}, \quad (2a)$$

$$(1/m_n^*)dF_n/dx = (1/m_{n+1}^*)dF_{n+1}/dx, \quad (2b)$$

where  $F_n$  is the wave function in each segment  $n$ , and  $m_n^*$  is the effective mass in each segment. The wave function in each segment can then be represented as the sum of forward and backward propagating exponential wave functions.<sup>1,10</sup> The determination of  $|T(E_x, V)|^2$  is then performed by a straightforward multiplication of  $2 \times 2$  matrices.<sup>1,10</sup>

The resulting transmission coefficients must be integrated as in Eq. (1). We do this integration numerically on a minicomputer. The upper limit of this integration can be chosen so that thermionic emission effects from the tail of the Fermi distribution are automatically included in the results. We assume that the electrons are launched from the contact region, thus implicitly assuming coherent transport between the heavily doped contact layer and the heterobarsriers. This assumption restricts application of this model to cases where the accumulation layer and the "potential hill" shown in Fig. 1 are small. Specifically, we only model devices which have contact doping concentrations of at least  $2 \times 10^{17} \text{ cm}^{-3}$  and to have undoped or lightly doped spacers on the cathode side of the device of 150 Å or less.

In other cases, the electron-launching assumptions need to be modified, resulting in changes to the valid values of  $E_f$  and  $T$ . Equation (1) would require rederivation if the injection is two dimensional, or if equilibrium Fermi statistics are no longer a good approximation. The other cases, in general, are not trivial, and are beyond the scope of this work.

One complication that arises in the determination of  $|T(E_x, V)|^2$  by this method is band nonparabolicity. In the GaAs/AlAs system, a completely imaginary component of the  $E$ -vs- $k$  relation connects the bottom of the electron conduction band with the light-hole valence band. The resulting dispersion relation for tunneling electrons is given by

$$E = E_0 \pm \hbar^2 Y (k^2 + Y^2)^{1/2} / m_{\pm}, \quad (3)$$

where

$$E_0 = E_c - E_{\text{gap}} / (1 + m_+ / m_-),$$

$$Y = \{E_{\text{gap}} / [\hbar^2 (1/m_+ + 1/m_-)]\}^{1/2},$$

$E_{\text{gap}}$  is the energy gap, and  $m_+$  and  $m_-$  are the conduction- and valence-band effective masses, and  $\hbar$  is the reduced Planck constant, respectively.<sup>12</sup> Nonparabolicity in the real part of the conduction band can be treated using a three-band model from  $k \cdot p$  theory:

$$E(K) = (\hbar k)^2 (1 - ak^2) (2m^*)^{-1}, \quad (4)$$

where  $a$  can be calculated using either Kane's model,<sup>13</sup> or by an empirical fit to the band structure. In this work, however, we use a parabolic conduction band ( $a = 0$ ) for computational simplicity.

The introduction of nonparabolic dispersion relations is not consistent with the use of the exponential propagating functions solutions in the effective-mass approximation

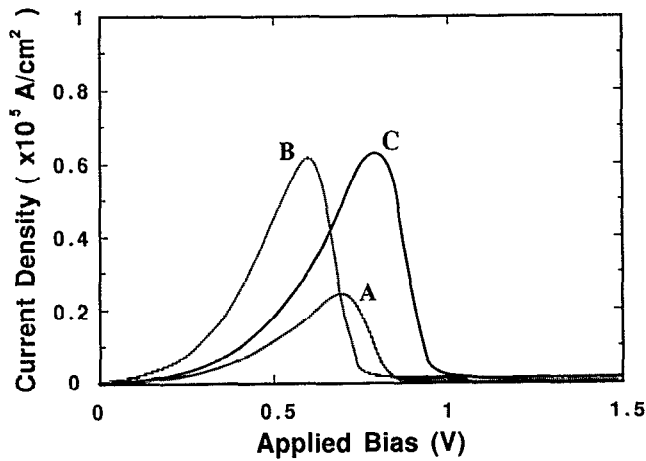


FIG. 2. Comparison of calculated  $I$ - $V$  curves with (curve C) and without (curve A) the local parabolic approximation for device (i) (see Table I and Fig. 5). Calculated  $I$ - $V$  characteristics using the nonparabolic imaginary wave vector and the conduction-band minimum effective mass are shown for comparative purposes (curve B).

as these solutions are based on the assumption of a parabolic dispersion relation. In order to accommodate this discrepancy, we replace both the effective mass and the wave vector in the envelope function matching conditions [Eq. (1)]. The nonparabolic wave vectors found in Eqs. (3) and (4) are substituted where appropriate for the parabolic wave vectors. The effective mass is replaced by

$$m^*(E) = (\hbar k')^2 / (2|E - E_c|) \quad \text{for } E > E_0 \quad (5a)$$

$$m^*(E) = (\hbar k')^2 / (2|E_v - E|) \quad \text{for } E < E_0, \quad (5b)$$

where  $k'$  is the wave vector found from the appropriate dispersion relation. By making these substitutions we are replacing the nonparabolic band structure with parabolic bands that vary with the electron energy. This local parabolic approximation (LPA) allows the accommodation of the effective mass envelope functions,<sup>1,10</sup> and a nonparabolic dispersion relation.

Current-voltage characteristics calculated using the LPA tend to have much higher-current densities, and better agreement with calculated results, than the strict parabolic approximation. The difference becomes more significant for higher potential barriers, which have a greater difference from a parabolic dispersion relation near the energy of the conduction-band minimum of the contacting potential. Figure 2 shows  $I$ - $V$  curves calculated using the parameters for device (i) from the next section of this paper. Comparing the results of Fig. 2 with Table I shows the improved agreement obtained by using the LPA; even better agreement can be obtained by comparing the "available current density,"  $J_p - J_v$ . It must be noted, however, that we can give no justification for this approach beyond the fact that it converges to the effective-mass approximation for electron energies near the bottom of the conduction band, and the substantial improvement in agreement with experimental results that we obtain.

TABLE I. Calculated and actual peak current densities (PCDs) for the devices used in this experiment. Also, measured available current densities (ACD),  $J_p - J_v$ , are shown.

Device	Predicted PCD (kA cm <sup>-2</sup> )		Measured PCD (kA cm <sup>-2</sup> )		ACD (kA cm <sup>-2</sup> )
	77 K	300 K	77 K	300 K	300 K
(i)	70	63	150 ± 10	140 ± 10	70 ± 10
(ii)	120	100	280 ± 20	250 ± 20	110 ± 20
(iii)	160	140	220 ± 20	200 ± 20	80 ± 20

We compare the predicted current densities of this model with various published results in Fig. 3, and see that the resonant current densities agree within a factor of 2.5 for current densities between  $2 \times 10^3$  and  $2 \times 10^5$ . This agreement is reasonable considering the fact that it corresponds to a one monolayer change in barrier thickness.<sup>14,15</sup> Effects of band bending due to the charge of the electrons in the quantum well have not been included in this model (self-consistency of the Schrödinger and Poisson equations), and may account for some of the difference with the experimental results. Including the effect of charge in the well would tend to increase the transparency of the second tunneling barrier to tunneling electrons, and the predicted current density.

The dependence of the measured  $I$ - $V$  curve on the parameters of the quantum region can be understood by comparing the computed full width at half maximum (FWHM) and resonant voltages of the transmission functions for a variety of double-barrier structures. Increasing the FWHM of the transmission resonance increases the peak current density<sup>16</sup> as long as the FWHM  $< (E_f - E_c)$ ; this can be seen from a careful inspection of Eq. (1) or its low-temperature limit.<sup>1</sup> Computed values of the FWHM of the transmission resonance are shown in Fig. 4, assuming simple rectangular barrier and well structures with no ap-

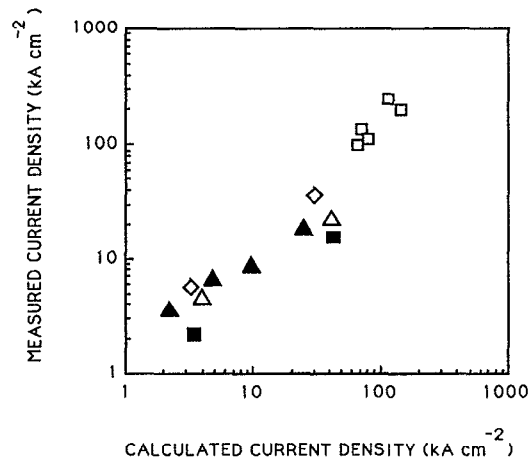


FIG. 3. Predicted resonant current density is compared with experimental results. The empty squares are for this paper and Ref. 20, solid triangles are from Ref. 22, solid squares are from Ref. 16, empty triangles are from Refs. 9 and 15, and the empty diamonds are from Ref. 22.

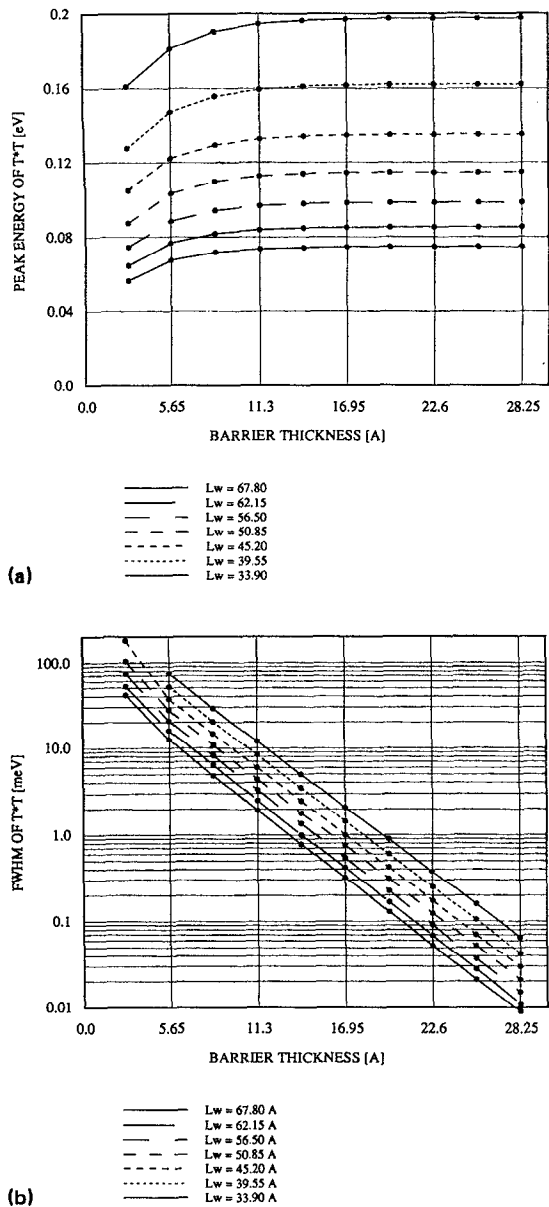


FIG. 4. Calculated peak energy (a), and full width at half maximum (FWHM) (b), of the transmission resonance are shown as a function of barrier thickness and well width for double-barrier resonant tunneling diodes in the AlAs/GaAs material system. From top to bottom the dashed and solid lines represent well widths of 33.9, 39.6, 45.2, 50.9, 56.5, 62.2, and 67.8 Å, respectively.

plied bias. The FWHM of the transmission resonance can be seen to vary strongly with both well and barrier thickness, resulting in a strong variation of the calculated resonant current. This strong variation in peak current density with well and barrier thickness has been confirmed experimentally.<sup>14,16</sup>

The resonant energy in conjunction with the voltage drops in the regions surrounding the heterobarriers, helps determine the bias at the peak current condition. In general, decreasing the well width increases the resonance energy and the amount of bias needed to achieve a current peak.

We do not compare the results of the “valley current” with this model, as only a tiny fraction of this current is predicted. This is because the mechanisms which cause such currents in the region past resonance are not included in this model.<sup>9,15,17</sup> These effects are not yet fully understood and are very difficult to compute, so we consider the origins of such currents when designing RTDs, but do not calculate them explicitly. In general, the same conditions which can break down the applicability of the coherent model also degrade the peak-to-valley ratio of the device. As an example of this, we know that  $X$ - $\Gamma$  valley scattering and interface roughness scattering<sup>17</sup> become serious for well widths on the order of 40 Å, so narrow wells result in poor device characteristics and are not advisable. In addition, the formation of an accumulation layer before the device is usually not desirable, as discussed previously, and can be suppressed by the use of doping modulation and/or band-gap engineering. Finally, ionized impurity scattering has been found to increase the valley current,<sup>9</sup> thus it is desirable to keep the layers closest to the quantum region undoped or very lightly doped.

### III. HIGH-CURRENT DEVICES

By using the transport model outlined in the previous section, we designed the epitaxial layers of three wafers (i), (ii), and (iii) for the fabrication of resonant tunneling diodes with high peak current densities and a low capacitance per unit area. The quantum well and barriers were chosen to be 45 and 17 Å, respectively in wafer (i), 51 and 14 Å, respectively, in wafer (ii), 45 and 14 Å respectively, in wafer (iii). AlAs barriers were used to reduce alloy scattering which may result from using  $\text{Al}_x\text{Ga}_{1-x}\text{As}$  barriers. Additionally, higher thinner barrier layers have a lower thermal component to the valley current than low thick barriers with similar current densities.<sup>18</sup> Predicted 300-K current densities ranging from  $6.3 \times 10^4$  for device (i), through  $1.4 \times 10^5$  for device (iii), were calculated using the coherent transport model described in the previous section.

The three wafers were grown by molecular-beam epitaxy (MBE) in a modified Varian Gen II (Ref. 19) on semi-insulating GaAs substrates. The GaAs growth rate was determined to be  $0.7 \mu\text{m/h}$  and the AlAs growth rate was set at  $0.3 \mu\text{m/h}$  by using beam flux calibration. A 5000-Å GaAs buffer layer doped  $2.5 \times 10^{18}$  was grown first, followed by a 400-Å layer where the doping was thermally graded down to  $2.0 \times 10^{17}$ . A subsequent 600-Å layer of  $2 \times 10^{17}$  material was used to reduce the voltage drop across the device while keeping the capacitive planes far apart. Undoped spacer layers of 100 Å were used on each side of the quantum region to reduce ionized impurity scattering, and to reduce the cathode side accumulation layer as shown in Fig. 1. Growth was interrupted at each heterointerface for 20 s to smooth the layers and to reduce interface scattering. The layers of the quantum region where chosen as described above. The cathode doping was set at  $10^{18}$  for 800 Å, and was thermally graded up to  $2 \times 10^{18}$  for a 4000-Å heavily doped capping layer.

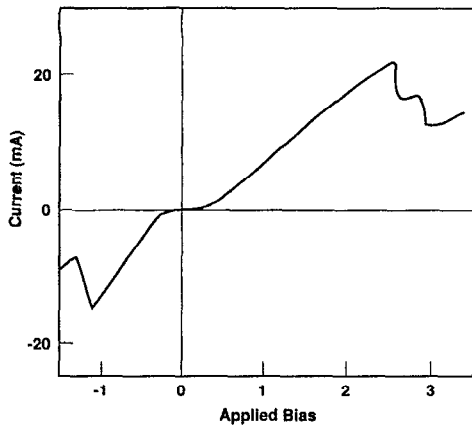


FIG. 5. Experimental  $I$ - $V$  curve is shown for a device from wafer (i) at room temperature. This device displays a PVR of 1.7 with a peak current density of  $1.4 \times 10^5$ .

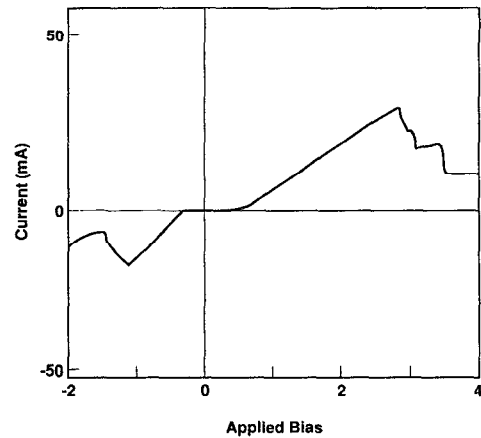


FIG. 7. An experimental current voltage curve is shown for a  $3 \times 5 \mu\text{m}$  device from wafer (iii) at 77 K.

Devices were fabricated by using a wet etch to isolate in one direction and ion implantation to isolate in the other direction.<sup>20</sup> Both the top and bottom ohmic contacts were made by using a Ni-Au-Ge alloy. Ti-Au interconnect metal over  $1 \mu\text{m}$  thick, intended for microwave measurements, aided in contacting the devices and also served as a heat sink. Devices with the top contacted by interconnect metal from two sides had the best current-voltage characteristics, resulting from more effective heat dissipation. At least 10 of these devices from each wafer were bonded for four-point-probe measurements at room temperature and 77 K.

Typical best current-voltage characteristics for these devices are shown in Figs. 5, 6, and 7. These devices displayed average room temperature current densities of  $1.4$ ,  $2.5$ , and  $2.0 \times 10^5$  for devices (i), (ii), and (iii), respectively. These results were found by averaging the current densities of several devices and plotting current versus

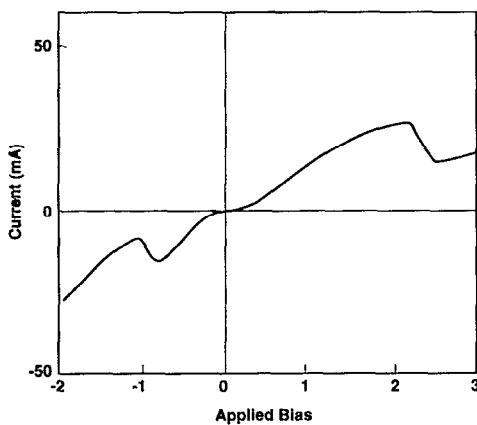


FIG. 6. An experimental  $I$ - $V$  curve is shown for a device from wafer (ii) with a PVR of 1.8 and a nominal area of  $1 \times 5 \mu\text{m}$  at room temperature. Comparison of peak current densities for several device sizes on this wafer at 77 K yield an average PCD of  $2.8 \times 10^5$  at 77 K and  $2.5 \times 10^5$  at room temperature. Based on the data for average peak current density, the actual size of this particular device is probably larger than the nominal area due to photolithographic overdevelopment.

nominal device area to eliminate systematic shifts in device size due to processing. The measurements were made using the "short" integration time on an HP4145, thus these results are similar to pulsed conditions. Typical best peak-to-valley ratios at room temperature (77 K) were 2.0 (3.3), 1.8 (3.1), and 1.7(3.0) for devices (i), (ii), and (iii), respectively. Devices with peak currents of over 25 mA tended to break down at room temperature due to thermal runaway. The improved stability at 77 K allowed us to confirm the current densities by measuring a larger set of device sizes (we corrected for the increase in current density with reduced temperature). These are the highest current densities ever measured for RTDs in the GaAs/AlAs system which showed a discernible NDR region at room temperature. Additionally, these results also include the highest difference of  $J_p$  and  $J_v$  in this material system, this difference being critical in the figure of merit for switching applications.<sup>7</sup>

The rough agreement between the predicted and observed PCDs show that the coherent model can serve as a helpful guide in designing RTDs with barriers as thin as five monolayers. The agreement improves when available current density, that is  $J_p - J_v$  is compared, as shown in Table I. The difference between the predicted trend of monotonically increasing PCDs and the observed results could be due to changes of 10% in either the Al or Ga flux rates in the MBE chamber, or a complimentary change totalling this amount. Measured changes in the flux rates before and after each growth were as much as 5% for the Ga and 10% for Al; the flux rates could not be measured during growth. This uncertainty in the growth rate can account for the discrepancy between predicted and measured PCDs for devices (i), (ii), and (iii).

The predicted and observed resonant voltages differed by roughly 1.4 V, this can be explained by a relatively high series resistance. The series resistance is largely due to vertical confinement of the anode current within the  $0.5\text{-}\mu\text{m}$ -doped bottom buffer, and the horizontal confinement from the ion implantation isolation. For the devices shown in Figs. 5, 6, and 7; the implantation confinement

was between 1 and 3  $\mu\text{m}$  wide, on a stripe 5  $\mu\text{m}$  long defined by mesa etching.<sup>20</sup> Including the local heating effects,<sup>21</sup> the center of the mesa can have as much as 25  $\Omega$  of anode resistance with 2- $\mu\text{m}$  horizontal confinement. This series resistance is a serious limitation for practical implementation of these devices for oscillator applications, and it contributes substantially to the heating and breakdown of these devices. Future changes in the processing technology, including thicker heavily doped buffer layers under the active region, better ohmic contacts, lower isolation implant dosages, and changes in the device layout could all contribute to lower series resistance effects.

#### IV. SUMMARY

We have described the design, fabrication, and measurement of GaAs/AlAs RTDs with the highest  $J_p - J_v$  to date using a planar process. A coherent transport model was described, and agreement was shown with a body of experimental data which satisfied the initial assumptions made in the model. The model was then used to design the epitaxial layers for resonant tunneling diodes which showed peak current densities as high as 2.5 (2.8) and peak to valley current ratios of 1.8 (3.0) at room temperature (77 K). The PCDs of these devices agree with the coherent model within a factor of 2.5, similar to the agreement shown with other published data, and within the inherent uncertainties of MBE growth.

#### ACKNOWLEDGMENTS

We are indebted to E. R. Brown for many useful discussions, encouragement, and providing Fig. 4. We are also grateful to E. C. Larkins for his guidance in the MBE growth; and K. L. Lear, M. J. W. Rodwell, Y. C. Pao, E. S. Hellman, and W. S. Lee for useful discussions. In addition, E. W. wishes to thank T. Narusawa, T. Onuma, T. Kajiwara, T. Fujita, and S. Moriyama for allowing him to

complete the writing of this work at Matsushita Opto-Electronics Research Laboratories. This work was supported under grant from the Defence Advanced Research Projects Agency (DARPA) N00014-84-0077 and the Office of Naval Research (ONR) N00014-85-0530.

- <sup>1</sup>R. Tsu and L. Esaki, *Appl. Phys. Lett.* **24**, 593 (1974).
- <sup>2</sup>L. L. Chang, L. Esaki, and R. Tsu, *Appl. Phys. Lett.* **24**, 593 (1974).
- <sup>3</sup>T. Inata, S. Muto, Y. Nakata, S. Sasa., T. Fujii, and S. Hiyamizu, *Jpn. J. Appl. Phys.* **26**, L1332 (1987).
- <sup>4</sup>T. P. E. Broekaert, W. Lee, and C. G. Fonstad, *Appl. Phys. Lett.* **53**, 1545 (1988).
- <sup>5</sup>C. I. Huang, M. J. Paulus, C. A. Bozada, S. C. Dudley, K. R. Evans, C. E. Stutz, R. L. Jones, and M. E. Cheney, *Appl. Phys. Lett.* **51**, 121 (1987).
- <sup>6</sup>J. R. Sonderstrom, D. H. Chow, and T. C. McGill, *Appl. Phys. Lett.* **55**, 1094 (1989).
- <sup>7</sup>S. K. Diamond, E. Ozbay, M. J. W. Rodwell, D. M. Bloom, Y. C. Pao, and J. S. Harris, Jr., *Appl. Phys. Lett.* **52**, 2163 (1988).
- <sup>8</sup>E. R. Brown, W. D. Goodhue, and T. C. L. G. Sollner, *J. Appl. Phys.* **64**, 1519 (1988).
- <sup>9</sup>E. Wolak, K. L. Lear, P. M. Pitner, E. S. Hellman, B. G. Park, T. Weil, and J. S. Harris, Jr., *Appl. Phys. Lett.* **53**, 201 (1988).
- <sup>10</sup>A. Harwit, Ph.D. thesis, Stanford University, 1987.
- <sup>11</sup>M. S. Lundstrom and R. J. Schuelke, *IEEE Trans. Electron Devices* **ED-30**, 1151 (1983).
- <sup>12</sup>J. N. Schulman and T. C. McGill, *Phys. Rev. B* **23**, 4149 (1981).
- <sup>13</sup>T. Hiroshima and R. Lang, *Appl. Phys. Lett.* **49**, 456 (1986).
- <sup>14</sup>M. A. Reed, W. R. Frensley, W. M. Duncan, R. J. Mayti, A. C. Seabaugh, and H. L. Tsai, *Appl. Phys. Lett.* **54**, 1256 (1989).
- <sup>15</sup>E. Wolak, Ph.D. thesis, Stanford University, 1989.
- <sup>16</sup>M. Tsuchiya and H. Sakaki, *Appl. Phys. Lett.* **49**, 88 (1986).
- <sup>17</sup>H. Sakaki, T. Noda, K. Hirakawa, M. Tanaka, and T. Matsusue, *Appl. Phys. Lett.* **51**, 1934 (1987).
- <sup>18</sup>M. Tsuchiya and H. Sakaki, *Appl. Phys. Lett.* **50**, 1503 (1989).
- <sup>19</sup>E. C. Larkins, E. S. Hellman, D. G. Schlom, J. S. Harris, Jr., M. H. Kim, and G. E. Stillman, *Appl. Phys. Lett.* **49**, 391 (1986).
- <sup>20</sup>S. K. Diamond, E. Ozbay, M. J. W. Rodwell, D. M. Bloom, Y. C. Pao, E. Wolak, and J. S. Harris, *Electron Device Lett.* **10**, 104 (1989).
- <sup>21</sup>K. H. Nichols, C. M. L. Yee, and C. M. Wolfe, *Solid-State Electron.* **23**, 109 (1980).
- <sup>22</sup>S. Muto, T. Inata, H. Ohnishi, N. Yokayama, and S. Hiyamizu, *Jpn. J. Appl. Phys.* **25**, L577 (1986).
- <sup>23</sup>E. R. Brown, T. C. L. G. Sollner, W. D. Goodhue, and C. D. Parker, *Appl. Phys. Lett.* **50**, 83 (1987).